This article was downloaded by:
On: *25 January 2011*
Access details: *Access Details: Free Access*
Publisher *Taylor & Francis*
Informa Ltd Registered in England and Wales Registered Number: 1072954 Registered office: Mortimer House, 37-41 Mortimer Street, London W1T 3JH, UK

Liquid Crystals
Publication details, including instructions for authors and subscription information:
http://www.informaworld.com/smpp/title~content=t713926090

Oscillating Poiseuille flow in photo-aligned liquid crystal cells

Sergey Pasechnik[a]; Ildar Nasibullayev[b]; Dina Shmeliova[a]; Valentin Tsvetkov[a]; Liu Zhijian[c]; Vladimir Chigrinov[c]
[a] Moscow State Academy of Instrument Engineering & Computer Science, 107846 Moscow, Russia [b] Institute of Mechanics, Ufa Research Center RAS, 450000 Ufa, Russia [c] Hong Kong University of Science & Technology, Clear Water Bay, Kowloon, Hong Kong

To cite this Article Pasechnik, Sergey , Nasibullayev, Ildar , Shmeliova, Dina , Tsvetkov, Valentin , Zhijian, Liu and Chigrinov, Vladimir(2006) 'Oscillating Poiseuille flow in photo-aligned liquid crystal cells', Liquid Crystals, 33: 10, 1153 — 1165
To link to this Article: DOI: 10.1080/02678290600965457
URL: http://dx.doi.org/10.1080/02678290600965457

PLEASE SCROLL DOWN FOR ARTICLE

Full terms and conditions of use: http://www.informaworld.com/terms-and-conditions-of-access.pdf

This article may be used for research, teaching and private study purposes. Any substantial or systematic reproduction, re-distribution, re-selling, loan or sub-licensing, systematic supply or distribution in any form to anyone is expressly forbidden.

The publisher does not give any warranty express or implied or make any representation that the contents will be complete or accurate or up to date. The accuracy of any instructions, formulae and drug doses should be independently verified with primary sources. The publisher shall not be liable for any loss, actions, claims, proceedings, demand or costs or damages whatsoever or howsoever caused arising directly or indirectly in connection with or arising out of the use of this material.

Liquid Crystals, Vol. 33, No. 10, October 2006, 1153–1165

Taylor & Francis
Taylor & Francis Group

Oscillating Poiseuille flow in photo-aligned liquid crystal cells

SERGEY PASECHNIK†, ILDAR NASIBULLAYEV‡, DINA SHMELIOVA†, VALENTIN TSVETKOV†, LIU ZHIJIAN§ and VLADIMIR CHIGRINOV*§

†Moscow State Academy of Instrument Engineering & Computer Science, Stromynka 20, 107846 Moscow, Russia
‡Institute of Mechanics, Ufa Research Center RAS, K Marksa Str. 12, 450000 Ufa, Russia
§Hong Kong University of Science & Technology, Clear Water Bay, Kowloon, Hong Kong

(*Received 29 November 2005; in final form 15 July 2006; accepted 16 July 2006*)

We present an experimental study of thin liquid crystal (LC) layers under the action of a harmonically varied pressure gradient. Optical measurements were performed to register the linear oscillations of a nematic director related to homeotropic and homeoplanar (hybrid) initial states. In the latter case one of the inner surfaces of the rectangular channels was treated by ultraviolet light to provide a relatively weak planar anchoring. The optical response of hybrid and homeotropic LC cells under an oscillating pressure gradient was investigated in relation to on the amplitude and frequency of the pressure gradient. A hydrodynamic model is developed taking into account the LC polar anchoring strength and the surface viscosity responsible for a fast LC surface dynamics. Our estimates show that the thickness of the boundary layer corresponding to the surface viscosity does not exceed 10^{-6} m, and further experiments are needed with thinner LC cells and higher frequency oscillations to achieve a more precise value. An oscillating Poiseuille flow in the hybrid cell was found to be useful for characterizing elastic and viscous properties of a weakly anchoring LC surface layer in a fast surface dynamic process.

Downloaded At: 15:53 25 January 2011

1. Introduction

The properties of a surface liquid crystal (LC) layer are of great interest for both fundamental science and practical applications. Surface treatment used in the LC display industry provides both strong or weak anchoring of the LC director at the surface [1]. The weakly anchored surface has found a practical application in newly developed LC displays, e.g. bistable nematic displays, with breaking of the weak anchoring under the action of sufficiently strong electric fields [2]. The operation of these devices is strongly dependent on a dynamic behaviour of the LC surface layer. In general, a variety of physical properties of both isotropic and anisotropic liquids can be modified by the surface. In particular, transport processes such as diffusion can be slowed in thin nanometer layers of polar liquids and liquid crystals [3–5]. The motion of polymeric chains contacted with the surface LC layer and other processes in the LC–surface interface, can also modify the LC cell dynamic response [6–8]. This renders the dynamics of the surface LC layer more complicated than the well known bulk response.

Some phenomenological descriptions of LC surface dynamics have been proposed by a number of authors [6, 7, 9–12]. In particular, an extremely slow field induced motion (gliding) of the LC easy axes at the surface was studied at weakly anchored surfaces with different treatments [6, 8, 10, 11]. The proposed theoretical models [6, 9, 12] consider LC surface layers described by a surface director $\mathbf{n}_s$, which moves more slowly than the bulk director $\mathbf{n}_b$. The surface director produces an additional viscous moment interacting with the bulk director from the boundary layers, which modifies the dynamic response of the LC to the external force applied to the layer. Usually the value of this moment is described in terms of a so-called surface viscosity. The surface viscosity is responsible for the phase shift between the bulk $\mathbf{n}_b$ and surface $\mathbf{n}_s$ directors. This shift is in a microsecond range and can hardly be detected directly [13]. Certain experimental techniques [7, 14, 15] have therefore been proposed to obtain information about the fast surface dynamics and the corresponding values of the surface viscosity coefficients. The term 'fast surface dynamics' is used here to distinguish the difference between (a) the fast processes taking place in the surface LC layer due to the surface viscosity and (b) the slow gliding of the easy axis mentioned above. To the best of our knowledge the value of the surface viscosity has been estimated only in [15, 16].

*Corresponding author. Email: eechigr@ust.hk

Liquid Crystals
ISSN 0267-8292 print/ISSN 1366-5855 online © 2006 Taylor & Francis
http://www.tandf.co.uk/journals
DOI: 10.1080/02678290600965457

The fast LC surface dynamics must be determined from the physical properties of both the LC and the solid surface. A well controlled technique for the surface treatment should therefore be used for the purpose. In principle, a variety of photoaligned surfaces with different anchoring properties can be proposed for a study of the surface dynamics of liquid crystals [1, 17]. We recently studied slow surface dynamics on a photoaligned LC surface under the action of a strong electric field [11].

Electro-optical investigations of a weakly anchored LC surface layer may encounter problems, such as spatial non-uniformity of the electric field, back-flow effects, and non-linear distortion of strong electric fields in a highly anisotropic media [1]. Optical studies of oscillating shear flows were recently considered as an alternative method for the registration of fast surface dynamics under weak anchoring [18, 19]. Such a technique can be general for LC materials and surfaces of different types. We know only one experimental study, where the surface viscosity coefficient at a weakly anchoring surface of a defined type was estimated from Couette like flow [19]. Following this study, we now apply the technique of Poiseuille shear flow to study the dynamics of a weakly anchored LC layer prepared by photoalignment. We have previously used this technique to study linear and non-linear orientational transformations at a strong homeotropic anchoring [20–22], and now investigate its application to the investigation of the fast surface dynamics of a weakly anchored LC layer.

Downloaded At: 15:53 25 January 2011

2. Dynamics of a weakly anchored nematic LC layer

2.1. *General equations*

Let us consider a nematic layer of thickness d confined between two solid substrates. The origin of the Cartesian coordinate system is chosen at the layer centre, with the z-axis perpendicular to the layer. The oscillatory Poiseuille flow induced by pressure gradient $(\Delta p_0/\Delta x)\cos(\omega t)$ is applied along the x-axis. The geometry of the flow is shown in figure 1.

The solution of the nematodynamics equation (velocity **v** and director orientation **n**) depends on the coordinate z and time t:

$$v=(v_z, 0, 0),\ n=(n_x, 0, n_z). \tag{1}$$

The velocity component $v_z=0$ due to the incompressibility condition $\mathrm{div}\,\mathbf{v}=0$. In order to work with dimensionless variables we introduce a typical time – reverse flow frequency ω^{-1} and a typical distance, the LC layer thickness d. The complete set of dimensionless dynamical nematic equations may be written:

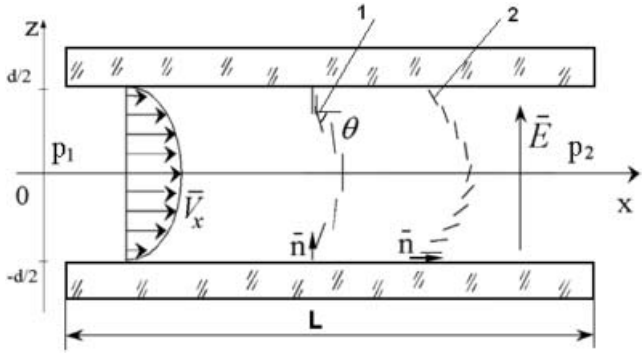

Figure 1. Flow geometry: the two types of initial orientation, homeotropic (1) and hybrid (2), are distorted by the pressure gradient $\Delta p/\Delta x=(p_2-p_1)/L$; the electric field **E** can be used for additional control of the orientation.

$$\varepsilon(n_x n_{z,zz}-k_{31}n_z n_{x,zz}+Fn_x n_z)+(n_z n_{x,t}-n_x n_{z,t}) + \frac{1}{\lambda-1}\left(n_z^2+\lambda n_x^2\right)v_{x,z}=0 \tag{2}$$

$$-a_p\cos t+\partial_z\left\{-n_z n_{x,t}-\lambda n_x n_{z,t}+ \frac{\alpha_4+(\alpha_3+\alpha_6)n_x^2+\left(\alpha_5-\alpha_2+2\alpha_1 n_x^2\right)n_z^2}{-2\alpha_2}v_{x,z}\right\}=0 \tag{3}$$

$$n_x^2+n_z^2=1 \tag{4}$$

where $\varepsilon=\frac{1}{\tau_d\omega}$, $\tau_d=\gamma_1 d^2/K_{11}$, $a_p=\frac{\Delta p_0}{\Delta x}\frac{d}{(-\alpha_2)\omega}$, $k_{31}=K_{33}/K_{11}$, $\lambda=\alpha_3/\alpha_2$, α_i is the Leslie viscosity, $\gamma_1=\alpha_3-\alpha_2$ is the rotational viscosity of a nematic, K_{ii} are the elastic constants.

Introducing a new variable θ, the angle between director orientation and the x-axis (figure 1) we can rewrite equation (1) in the following form:

$$n_x=\cos\theta(z,t),\ n_y=0,\ n_z=\sin\theta(z,t),\ v_x=v_x(z,t),\ v_y=0,\ v_z=0. \tag{5}$$

Thus normalization condition (4) is satisfied automatically and equations (2), (3) take the form:

$$\theta_{,t}-K(\theta)v_{x,z}=\varepsilon\left[P(\theta)\theta_{,zz}+1/2P'(\theta)\theta_{,z}^2+F\cos\theta\sin\theta\right] \tag{6}$$

$$-a_p\cos(\mathrm{t})+\partial_z\{-(1-\lambda)K(\theta)\theta_{,t}+Q(\theta)v_{x,z}\}=0 \tag{7}$$

with

$$K(\theta)=\frac{\lambda\cos^2\theta-\sin^2\theta}{1-\lambda},\ P(\theta)=\cos^2\theta+K_{31}\sin^2\theta,$$

$$Q(\theta)=\frac{\alpha_4+(\alpha_5-\alpha_2)\sin^2\theta+\left(\alpha_3+\alpha_6+2\alpha_1\sin^2\theta\right)\cos^2\theta}{2(-\alpha_2)},\quad F=\pi^2E^2/E_F^2, \tag{8}$$

$E_F=(\pi/d)[K_{11}/(\varepsilon_0\varepsilon_a)]^{\frac{1}{2}}$, ε_a is the LC dielectric anisotropy.

The boundary condition for the velocity field (no-slip) is

$$\mathbf{v}(z=\pm 1/2)=0. \tag{9}$$

We will examine the two types of the director boundary conditions: symmetrical (weak homeotropic or planar boundary alignment on both substrates) and hybrid (one substrate with strong homeotropical anchoring, the other with weak planar anchoring). The boundary condition for weakly anchored surfaces can be written as [13]:

$$\pm P(\theta)\theta_{,z}+\frac{1}{2}\frac{Wd\partial f_s}{K_{11}\partial\theta}+\frac{\omega d}{K_{11}}\eta_s\frac{\partial\theta}{\partial t}=0 \tag{10}$$

where W is the polar anchoring strength, $f_s(\theta-\theta_0)=\sin^2(\theta-\theta_0)$ is the function entering into the Rapini potential for specific surface energy per unit area, θ_0 is a preferred LC direction on the surface:

$$F_s=\left(1/2\right)Wf_s(\theta-\theta_0). \tag{11}$$

$\eta_s=\gamma_1\cdot l_{\gamma_1}$ is the so-called surface viscosity, which determines the viscous losses in the near-boundary layer of thickness l_{γ_1} [12–14]. The parameter l_{γ_1} can be considered as a characteristic length of a boundary layer, where the rotation viscosity γ_1 is modified by the higher order parameter near the solid surface [1]. In practice the particular type of boundary conditions is determined by a suitable surface treatment. For strong anchoring we have $\theta=const$ at the boundary (equal to zero for planar alignment and $\pi/2$ for homeotropic alignment).

Symmetrical boundary conditions are

$$\begin{aligned}&\mp P(\theta)\theta_{,z}+W_d\sin(\theta-\theta_0)\cos(\theta-\theta_0)+\eta_d\theta_{,t}\\&=0,\ '-'\text{ for } z=+1/2 \text{ and } '+' \text{ for } z=-1/2.\end{aligned} \tag{12}$$

In the hybrid cell we have:

$$\theta=\pi/2\big|_{z=+1/2}\ \text{(strong homeotropic anchoring)} \tag{13}$$

$$\begin{aligned}&-P(\theta)\theta_{,z}+W_d\sin(\theta)\cos(\theta)+\eta_d\theta_{,t}\\&=0\big|_{z=-1/2}\ \text{(weak planar anchoring)}\end{aligned} \tag{14}$$

where $W_d=dW/(K_{11})$, $\eta_d=d\gamma_1 l_{\gamma_1}\omega/(K_{11})$, and $W>0$.

2.2. *Symmetric boundary conditions*

In this section we present a brief review of the theoretical results previously obtained in [18], making use of the definitions of symbols and functions used in this study. Let us solve the set of equation (6) and (7) with the boundary conditions (9) and (12) with a constant average angle at the boundaries. For small flow amplitudes a_p we can expand the equations using small perturbations $\widetilde{\theta}$, $\widetilde{U}$ near the initial state θ_0, v_{0x}:

$$\theta=\theta_0+\widetilde{\theta},\ v_x=v_{x0}+U,\ \left|\widetilde{\theta}\right|\ll 1,\ |U|\ll 1,\ \partial f_s/\partial\theta=2\widetilde{\theta} \tag{15}$$

with boundary conditions

$$\begin{aligned}&U(z=\pm 1/2)=0,\quad \widetilde{\theta}_{,z}-E\widetilde{\theta}-G\widetilde{\theta}_{,t}=0\\&\big|_{z=-1/2},\quad \widetilde{\theta}_{,z}+E\widetilde{\theta}+G\widetilde{\theta}_{,t}=0\quad\big|_{z=+1/2},\\&E=dW/(P_0K_{11}),\ G=d\gamma_1 l_{\gamma_1}\omega/(P_0K_{11}),\ W>0\end{aligned} \tag{16}$$

and obtain the set of linear differential equations for small perturbations $\widetilde{\theta}$ and $\widetilde{U}$:

$$\begin{aligned}&\widetilde{\theta}_{,t}-K_0U_{,z}=\varepsilon\left(P_0\widetilde{\theta}_{,zz}+F\widetilde{\theta}\right),\\&-(1-\lambda)K_0\widetilde{\theta}_{,tz}+Q_0U_{,zz}=a_p\cos(t)\end{aligned} \tag{17}$$

where $P_0=P(\theta_0)$, $K_0=K(\theta_0)$, $Q_0=Q(\theta_0)$. The solution of equation (17) is expressed as:

$$\begin{aligned}&\widetilde{\theta}(z,t)=T_1(z)\cos(t)+T_2(z)\sin(t),\ U(z,t)\\&=U_1(z)\cos(t)+U_2(z)\sin(t)\end{aligned} \tag{18}$$

where:

$$\begin{aligned}&T_1(z)=-a_pM\left[\frac{(c_1+M_fc_2)f_1(z)-(c_2-M_fc_1)f_2(z)}{\left(1+M_f^2\right)(c_1^2+c_2^2)}-2M_fz\right]\\&M_f=\frac{\varepsilon FQ_0}{Q_0-(1-\lambda)K_0^2}\\&T_2(z)=-a_pM\left[\frac{(c_1+M_fc_2)f_2(z)+(c_2-M_fc_1)f_1(z)}{\left(1+M_f^2\right)(c_1^2+c_2^2)}-2z\right]\\&M=\frac{K_0}{2\left[Q_0-(1-\lambda)K_0^2\right]}.\end{aligned} \tag{19}$$

Here c_i are the coefficients which depend on W_d and η_d, f_i are the functions of z.

In case of strong surface anchoring ($E\gg 1$) the boundary conditions (16) become quite simple:

$$\widetilde{\theta}=0,\ z=\pm 1/2. \tag{20}$$

In this case the functions $\widetilde{T}_i(z)$ depend on the frequency of the oscillations through wave number dependence $k\sim\omega^{1/2}$. At a sufficiently high frequency the latter parameter defines the distortions of LC velocity and orientation in the LC surface layer. It is also true for weak anchoring if the viscous contribution to the boundary condition is essentially smaller than the elastic one:

$$v=G/E=\eta_s\omega/W<1. \tag{21}$$

It is easy to estimate the frequency $f_m=\omega_m/2\pi$ at which surface viscosity effects can play the most important

Downloaded At: 15:53 25 January 2011

role, by putting $v=1$. For $d=20\times10^{-6}$ m, $\eta_s=10^{-8}$ Pa s m, f_m varies from 15 to 150 Hz in the range of anchoring strength 10^{-6}–10^{-5} J m^{-2} [15, 16]. It was shown by computer modelling of the dynamical behavior of a homeotropic layer [18] that the surface viscosity can be estimated by analysing the frequency dependence of optical response at frequencies comparable with f_m. Indeed, the intensity I of light passed through the LC cell placed between crossed polarizers (oriented at 45° relatively the boundary planar orientation) can be expressed as:

$$I(t)=I_0\sin^2\frac{\delta(t)}{2} \tag{22}$$

where I_0 is the input light intensity, and δ is the optical phase delay between the extraordinary (e) and ordinary (o) rays with refractive indic n, defined as:

$$\delta(t)=\frac{2\pi d}{\lambda}\langle\Delta n(\theta)\rangle=\frac{2\pi}{\lambda}\int_{-d/2}^{d/2}[n(\theta)-n_0]\mathrm{d}z \tag{23}$$

$$n(\theta)=n_o\left[1-\cos^2\theta\left(n_e^2-n_o^2\right)/n_e^2\right]^{-1/2}. \tag{24}$$

Thus the flow-induced oscillations of the LC director orientation result in time changes of the optical phase delay and light intensity. In the case of the initial homeotropic state at $\delta<\pi$ the intensity of the light oscillates with double frequency, with the maximum value I_{max} depending on frequency (figure 2). Electric fields can also be useful in such a study as they provide a control of the spectra of director motion [21]. Figures 2 and 3 show the maximum of the light intensity vs. the flow frequency (figure 2) and external electric field intensity (figure 3) for different values of the surface

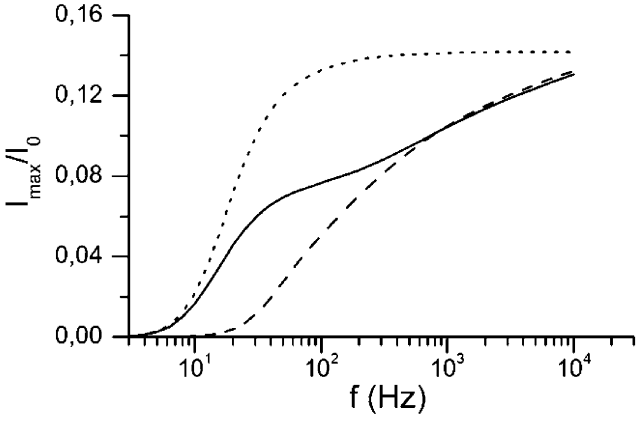

Figure 2. Maximum of light intensity vs. flow frequency. The parameters $a_p=0.2$, $d=10\,\mu$m, $W=10^{-6}$ J m^{-2}: dotted line, $l_{\gamma_1}=10^{-7}$ m; solid line, $l_{\gamma_1}=0$ m; dashed line, strong anchoring $W\to\infty$. Numerical calculations were made for the parameters of 5CB at 26°C.

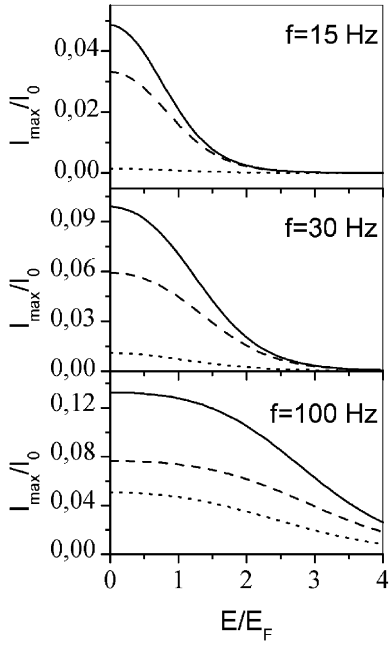

Figure 3. Maximum of light intensity vs. external electric field intensity. The parameters $a_p=0.2$, $d=10\,\mu$m, $W=10^{-6}$ J m^{-2}: solid line, $l_{\gamma_1}=0$ m; dashed line, $l_{\gamma_1}=10^{-7}$ m; dotted line, strong anchoring. Numerical calculations were made for the parameters of 5CB at 26°C.

viscosity. In these calculations the parameters of LC 5CB (*p*-pentylcyanobiphenyl) at 26°C were used [1, 22].

The influence of the surface viscosity is very strong in some region of the flow frequency ($f=10$–1000 Hz) or under an external stabilizing electric field (for the fixed flow frequency). Note that the field dependence I_{max}/I_0 (E/E_F) is more easily reproduced in experiment in comparison with the graph of figure 2.

2.3. *Hybrid boundary conditions*

We now consider the influence of weak anchoring on the orientational structure and optical properties of a hybrid (homeoplanar) layer. For the stationary case, in the absence of electric field and flow, the equation (6) for a director becomes relatively simple:

$$P(\theta)\theta_{,zz}+\left(1/2\right)P'(\theta)\theta_{,z}^2=0. \tag{25}$$

This equation has a simple solution in the case of the one-constant approximation ($K_{11}=K_{33}$):

$$\theta=C_1z+C_2 \tag{26}$$

where C_1 and C_2 are the constants to be determined from boundary conditions. For strong anchoring at both surfaces ($z=\pm1/2$) we obtain:

$$C_1=\pi/2,\ C_2=\pi/4. \tag{27}$$

Downloaded At: 15:53 25 January 2011

In the case of weak anchoring on the planar substrate these constants are determined from the following expressions:

$$C_2 = \pi/2 - C_1/2 \tag{28}$$

$$C_1 - (1/2)\chi^{-1}\sin(2C_1 d) = 0 \tag{29}$$

where the parameter

$$\chi = K_{11}/Wd \tag{30}$$

can be considered as a small parameter for the surfaces with relatively weak anchoring. For example, for $K_{11} = 8.5 \times 10^{-12}$ N, $d = 20 \times 10^{-6}$ m (typical parameters of our experiments), χ varies from 0.04 for $W = 10^{-5}$ J m^{-2} to 0.4 for $W = 10^{-6}$ J m^{-2}. In this case the expressions for C_1 and C_2 can be obtained from the first order expansion of equation (29):

$$C_1 = \pi/2(1-\chi),\ C_2 = \pi/4(1+\chi). \tag{31}$$

This results in a non-zero value for the polar angle on the weak anchoring plate:

$$\theta\left(z = -1/2\right) = \pi\chi/2. \tag{32}$$

We will simplify expression (23) taking into account that $(n_e - n_0)/n_e = \Delta n/n_e \ll 1$:

$$\begin{aligned}\delta &= \frac{2\pi d}{\lambda}\int_{-1/2}^{1/2} 1/2\left[n_0\left(n_e^2 - n_0^2\right)/n_e^2\right]\cos^2\theta(z)\mathrm{d}z \\ &\approx \frac{2\pi d}{\lambda}\int_{-1/2}^{1/2}\Delta n\cos^2\theta(z)\mathrm{d}z.\end{aligned} \tag{33}$$

Using equations (26) and (31) we can write the expression for δ as:

$$\delta_0 = \frac{2\pi d}{\lambda}\Delta n\left[1/2 - \chi/(1-\chi)\right]. \tag{34}$$

For a strongly anchored surface expression (34) becomes

$$\delta = \frac{\pi d}{\lambda}\Delta n \tag{35}$$

which means that the phase delay for homeoplanar (hybrid) orientation is half of that for a planar orientation.

It is convenient to use the reorientation of a hybrid cell under the action of an electric field to estimate the anchoring strength. In particular, for a LC with a positive dielectric anisotropy ε_a, the application of an electric field leads to a homeotropic orientation everywhere except in a thin boundary layer near a planar surface, and to a variation $\delta_h = \delta_0$ of the phase delay as determined by expression (34). If an electric field is applied to a LC with a negative ε_a, the variation δ_p of the phase delay is expressed as:

$$\delta_p = \frac{2\pi d}{\lambda}\Delta n_p[1/2 + \chi/(1-\chi)]. \tag{36}$$

For two LCs with different signs of ε_a but with identical anchoring and approximately the same values of Δn, the ratio

$$\delta_p/\delta_h = \frac{\Delta n_p[1/2 + \chi/(1-\chi)]}{\Delta n_h[1/2 - \chi/(1-\chi)]} \approx \frac{\Delta n_p}{\Delta n_h}(1+2\chi) \tag{37}$$

depends only on parameter χ, and can be used to estimate the anchoring strength W according to equation (30). In our experiments such a situation was realized by replacing the mixture with negative ε_a (ZhK440) by the same LC material slightly (12%) doped with a highly polar compound so that the obtained mixture showed a positive ε_a. The ratio $(\Delta n_p/\Delta n_h)$ for this case was measured to be 1.08 ± 0.02.

Let us consider the flow induced small deviations $\tilde{\theta}$ from the initial non homogeneous state approximately defined by expression (26). It is reasonable to propose that these deviations are proportional to the amplitude a_p of the driving force. Following equation (33) the optical phase delay can be expressed as:

$$\begin{aligned}\delta &= (2\pi d\Delta n/\lambda)\langle\cos^2\left[\theta_0(z) + \tilde{\theta}(z,t)\right]\rangle \\ &\approx (2\pi d\Delta n/\lambda)\langle\cos^2\theta_0(z) - \tilde{\theta}(z,t)\sin 2\theta_0(z)\rangle\end{aligned} \tag{38}$$

where <...> denotes mean value, $\theta_0(z)$ is the initial LC orientation determined from equation (26) and we assume $\tilde{\theta} \ll \theta_0$. In this case the flow-induced difference $\tilde{\delta}$, between the maximum δ_{max} and minimum δ_{min} value of δ, has to be proportional to a_p contrary to the quadratic dependence for a homeotropic LC sample. So we may expect that for a hybrid cell $\tilde{\delta}$ has to be proportional to the amplitude a_p of the driving force:

$$\tilde{\delta} \propto a_p \propto \frac{\Delta p_0}{\Delta x}T. \tag{39}$$

This result can be verified in experiment by analysing the intensity of a polarized light, passed through a hybrid LC cell. The coefficient of proportionality depends on the frequency, as in the case of symmetrical homeotropic anchoring. At a high frequency limit ($\varepsilon \ll 1$) the boundary layers become very thin and do not contribute to the phase delay changes. In a low frequency limit ($\varepsilon \gg 1$) the phase delay variations do not

Downloaded At: 15:53 25 January 2011

depend on frequency, and are defined only by the elastic surface contribution. Thus the intermediate frequency range $\varepsilon \sim 1$ appears the most useful for estimation of the surface viscosity.

We solved equations (6), (7) with boundary conditions (9), (13), (14) by a finite-difference method. After discretization the finite-difference equations were solved by a relaxation method. For the initial estimate a linear profile was chosen for the director alignment angle θ. Actually a linear solution corresponds to strong hybrid orientation without LC elastic anisotropy. It was shown by calculations that the nematic elastic anisotropy only slightly changed the linear solution. A weak anchoring solution can be dramatically different from the strong anchoring solution, but the relaxation scheme supplies a smooth convergence toward the desired solution.

Figure 4 shows the relaxation process of optical phase delay from the initial estimate to the correct solution (periodicity in time is the convergence criterion). In calculations we used the parameters of LC MBBA (4-methoxybenzylidene-4′-butylaniline) [1, 23, 24].

For weak anchoring (dashed line) the scheme relaxes to the new periodic solution (in three periods of the external flow). The dotted line corresponds to strong anchoring (fixed director orientation at the boundaries). We have phase oscillations due to the LC bulk director dynamics. The last case corresponds to high surface viscosity (solid line). Here we observe the slower relaxation from the initial estimate solution to the exact one. The high viscosity prevents fast orientational motion at the surface so the periodical solution (solid line) is harder to obtain than in the weak anchoring case.

The calculated dependence of flow-induced changes of the phase delay on the period T of pressure oscillations at different values of the anchoring energy W and a fixed value of surface viscosity is shown in figure 5. Increase of the anchoring strength results in rather complicated transformations of these dependences with the local slope of the curves variation within the range 1–1.5 for frequencies 1–10 Hz, while the relationship (39) describes the linear part of the curves.

Figure 6 shows the difference of the phase delay versus period T for fixed (weak) anchoring energy and different values of surface viscosity. There is little difference between $l_{\gamma 1}=10^{-7}$ m and $l_{\gamma 1}=10^{-6}$ m (weak anchoring) but above $l_{\gamma 1}=10^{-5}$ m the effect of the surface viscosity is most pronounced.

3. Experimental

3.1. *Liquid crystal cells*

The typical construction of the cells used in our experiments is shown in figure 7. The low frequency experiments in layers of MBBA confined by strongly anchored homeotropic surfaces were performed in wedge-like cells with a variable gap described previously in detail [25]. Hybrid cells with a constant gap were prepared by a photoalignment technique. In both cases, the two open edges of the cell are connected to the cylindrical tubes via intermediate channels of sufficiently large cross-section and low hydrodynamic resistance. A variable air pressure difference applied to

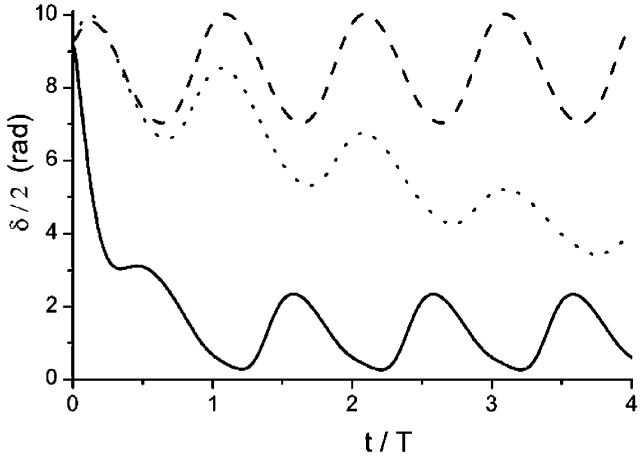

Figure 4. Computer simulation of the relaxation process in a homeoplanar (hybrid) cell. Optical phase delay δ vs. adjusted time: dashed line, weak anchoring, dotted line, strong anchoring; solid line, high surface viscosity. $d=20\,\mu$m, $\Delta p_0/\Delta x=10^3$ Pa m^{-1}. Calculations were made for the parameters of MBBA.

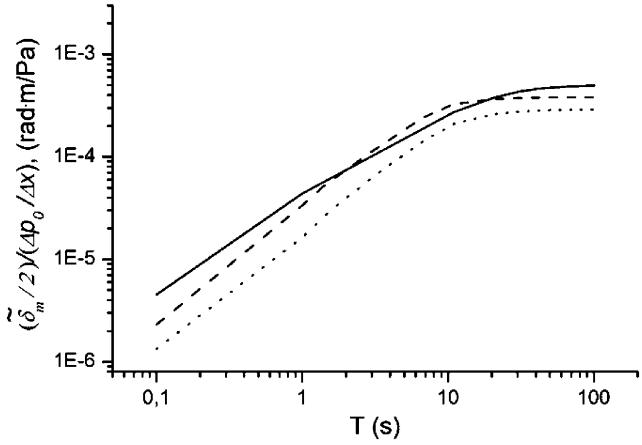

Figure 5. Numerical simulation of the normalized difference of phase delay $\tilde{\delta}_m/2$ in a homeoplanar layer of MBBA vs. the period of pressure oscillations T. The parameters $l_{\gamma_1}=10^{-6}$ m, $d=20\,\mu$m, $\Delta p_0/\Delta x=10^3$ Pa m^{-1}: solid line, $W=10^{-7}$ J m^{-2}; dashed line, $W=10^{-5}$ J m^{-2}; dotted line, $W=10^{-6}$ J m^{-2}.

Downloaded At: 15:53 25 January 2011

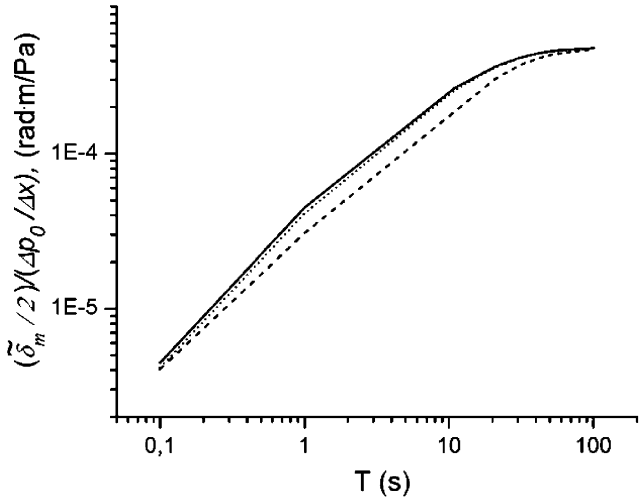

Figure 6. Numerical simulation of the normalized difference of phase delay $\tilde{\delta}_m/2$ in a homeoplanar layer of MBBA vs. period of pressure oscillations T. The parameters $W=10^{-7}\,\mathrm{J\,m^{-2}}$, $d=20\,\mu\mathrm{m}$, $\Delta p_0/\Delta x=10^3\,\mathrm{Pa\,m^{-1}}$: solid line, $l_{\gamma_1}=10^{-7}\,\mathrm{m}$; dotted line, $l_{\gamma_1}=10^{-6}\,\mathrm{m}$, dashed line, $l_{\gamma_1}=10^{-5}\,\mathrm{m}$.

the free LC surfaces in the tubes is transmitted to the thin LC layer in the thin central rectangular channel with no pressure loss. We used rather short (3–10 mm) central channels to obtain high pressure gradients at relatively low pressure differences (up to 300 Pa) applied to the layer. The central part of the hybrid cell was formed by two glass plates with inner surfaces treated in a special manner to provide a hybrid orientation. One of the surfaces was coated by chrome distearyl film to obtain strong homeotropic anchoring. The opposite surface was spin-coated with a 0.5% dye solution (sulphuric dye SD1) in *N*,*N*-dimethylformamide (DMF) and illuminated by UV polarized light ($\lambda=360\,\mathrm{nm}$ and $I_{uv}=0.8\,\mathrm{mW\,cm^{-2}}$) by a standard method [17]. The cell was separated into different zones treated with UV light for different exposure times (t_{ex}). Usually, such a procedure provides a different degree of orientational order in a photosensitive layer and various anchoring strengths (at least, for azimuthal anchoring [6]).

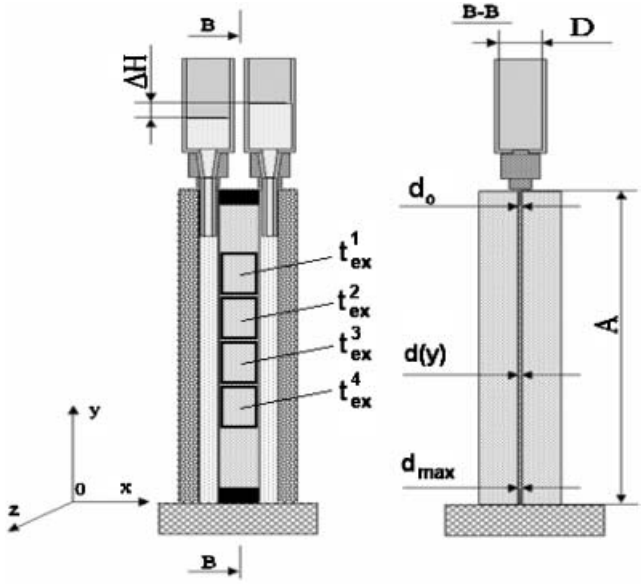

Figure 7. Typical construction of a liquid crystal cell: d, A, L are the geometrical sizes of the channel; for a wedge-like cell $d=d(y)$; the diameter D of the open tubes is large enough to avoid a hydrostatic pressure difference ΔH at low frequency measurements; t^i_{ex} correspond to different exposure times of UV treatment.

3.2. *Experimental set-up*

The general scheme of the experimental set-up is shown in figure 8. The low frequency (<1 Hz) variable pressure difference applied to the LC layer was generated by the special mechanical system described previously [21], based on the regulated compression of air in the cylinder. In case of the higher frequencies (5–30 Hz) this system was replaced by one using the air compression in a silphon. The regulation of pressure in these systems was achieved both by changing the amplitude of mechanical vibrations and by the application of capillaries of different length and diameter, which connected both sides of the cell and the entire aerodynamic system with the environment. We thus minimized extremely slow (<0.01 Hz) variations of the pressure difference applied to the LC layer induced by thermal instabilities of different parts of the system. This arrangement excluded the precise choice of the null position of the mechanical system, which plays a key role in the analogous system without capillaries [26].

The optical part of the experimental set-up was traditional for a polarized optical investigation. We registered simultaneously the time variations of the intensity $I(t)$ of polarized light passed through the cell and the time dependences Δp(t) of the pressure difference applied to the liquid crystal layer. The cell was placed between crossed polarizers at an angle $\beta=45^\circ$ with respect to the flow direction (geometry 'a'). In this case the maximum amplitude of the flow-induced light intensity was observed. In these experiments a high frequency (3 kHz) electric field was applied to the layer.

Measurement of the phase delay variations induced by an electric field in samples with a similar composition but with opposite sign of LC dielectric anisotropy ε_a, allowed us also to estimate the LC anchoring energy (see below).

Downloaded At: 15:53 25 January 2011

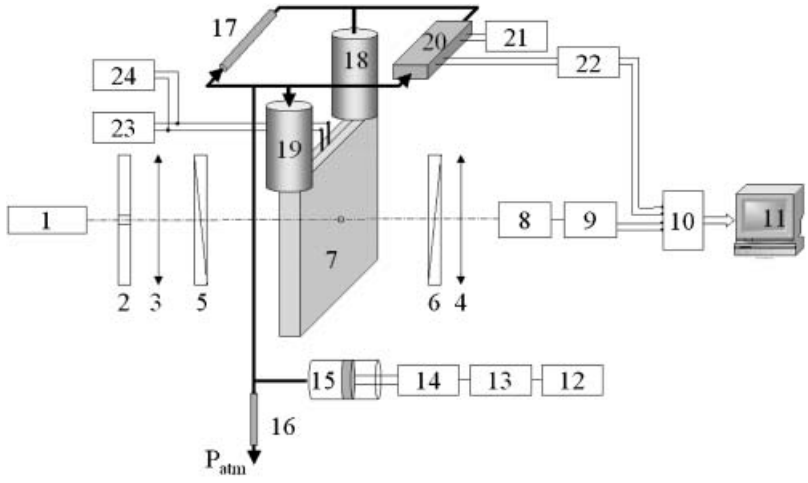

Figure 8. Experimental set-up: 1, He-Ne laser; 2, diaphragm, 3,4, lenses; 5,6, polarizers; 7, LC cell; 8, photodiode; 9, amplifier; 10, AD converter; 11, computer; 12–15, mechanical system for air pressure supply; 16,17, capillaries, 18,19, tubes partly filled with LC; 20,21,22, pressure sensor with electric supply and amplifier; 23, a.c. generator; 24, voltmeter.

Downloaded At: 15:53 25 January 2011

3.3. *LC materials*

Two nematic LC mixtures ZhK440 ($\varepsilon_a=-0.4$) and ZhK616 ($\varepsilon_a=+3.5$) produced by NIOPIK were used in the experiments. The first mixture consists of the well studied mesogenic compound: 4-*n*-butyl-4-methoxyazoxybenzene (N4) and *n*-butyl-4-heptanoyloxyazoxybenzene (2:1); the second mixture includes additionally a polar component (4-cyanophenyl ether of *n*-heptylbenzoic acid) with the concentration 2:10:5 relative to the first and second components. Such a weak doping can produce only slight changes in all the material parameters except the LC dielectric anisotropy ε_a. This was confirmed by analysis of the low frequency data previously obtained for homeotropic samples of these mixtures in cells with similar construction and strong anchoring [21]. We also used a well known nematic LC, MBBA (4-methoxybenzylidene-4′-butylaniline) for quantitative comparison with the theoretical predictions involving hybrid cells, as described above.

4. Results and discussion

4.1. *Electric field without flow: control of thickness and polar anchoring energy*

According to the expressions (34)–(37) the local LC layer thickness can be controlled using the total changes of phase delay δ_t induced by a strong electric field applied subsequently to the cells with positive and negative signs of ε_a. For this type of measurement we took into account that the values of anisotropy of refractive index of the two mixtures are close to each other (the difference is no more than 10%). The unique assumption in this case is that the boundary orientation of a director is the same for both mixtures studied. In this case the local thickness of the LC layer can be calculated from the total change of phase delay $\delta_t=\delta_p+\delta_h$ as:

$$\delta_t=(2\pi d/\lambda)(\Delta n). \tag{40}$$

The values of δ_p and δ_h may be found by analysing the time dependence $I(t)$ of the intensity of polarized light, passed through the LC cell after switching off the electric field. Examples of such dependences obtained for the two mixtures studied are shown in figure 9.

The character of the optical response is usual for experiments of this type, performed in cells with strong anchoring. The analogous dependence $I(t)$ obtained for

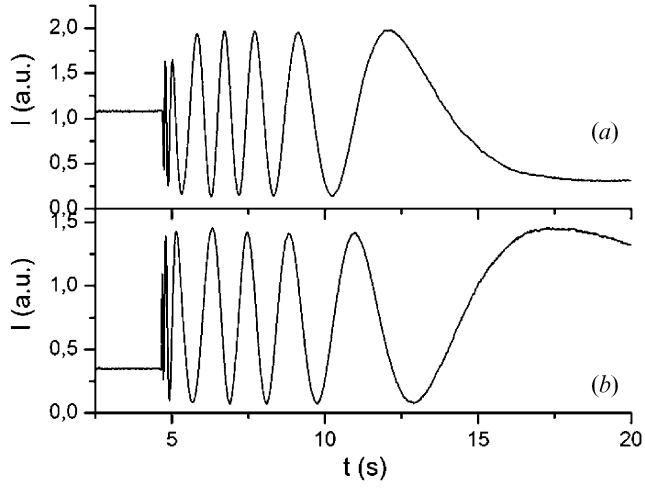

Figure 9. Light intensity $I(t)$ after turn off of electric field: $U=40$ V, $f=3$ kHz, $d=43.2$ μm, $t_{ex}=40$ min. (*a*) ZhK440, (*b*) ZhK616.

Table 1. LC cell phase variation and anchoring energy for various UV exposure times.

t_{ex}/min	$\delta_p/2$/rad (ZhK440)	$\delta_h/2$/rad (ZhK616)	δ_p/δ_h	χ	$W \times 10^{-6}\,J\,m^{-2}$
10	9.08	7.31	1.24	0.075	2.7 ± 0.2
20	9.78	8.60	1.14	0.022	8 ± 2
30	10.6	9.45	1.12	0.018	9 ± 3
40	8.57	8.24	1.04	0.0	$\geqslant 20$

a different orientation of the cell (geometry 'b', the polarization axis of the polarizer is parallel/normal to the LC director plane, analyser crossed with a polarizer) shows no visible transformations of the light intensity curves. This confirms that the director mostly moves in the plane defined by the easy axis on the photoaligned substrate. The latter differs from the case of a homeotropic LC layer with azimuthally degenerated orientation. Examples of the calculated phase delay variation and corresponding local LC layer thickness are presented in table 1 for different exposure times in a channel of relatively large thickness, $d=45\,\mu m$. The deviations of thickness ($\pm 5\,\mu m$) from the mean value $d=45\,\mu m$ are caused by the wide width ($A=3\,cm$) and short length ($L=3\,mm$) of the channel.

According to the simplified model described above we can use the data for δ_p and δ_h to estimate the anchoring energy. The experimental ratio δ_p/δ_h is very close to that predicted by the model expressions (34)–(37), for the case of strong anchoring in the region treated by UV light for a sufficiently long time. At the same time δ_p/δ_h increases with decreasing exposure time, which can be explained by a decrease of the LC anchoring energy. Estimated values of the anchoring energy are presented in table 1. The obtained data show that for low values of exposure time the planar surface anchoring orientation can be considered as a relatively weak one.

Thus in the framework of such approximation the results obtained can be used to estimate the value of the anchoring energy and its dependence on the time t_{ex} of UV illumination. Such estimates are presented in table 1. We see that anchoring energy varies in the range 10^{-6}–$10^{-5}\,J\,m^{-2}$, which corresponds to weak LC surface anchoring, and increases with the exposure time t_{ex} of UV illumination. Although such an increase is proved for the azimuthal LC anchoring energy it has to be specially verified in the case of polar LC anchoring energy [27].

4.2. *Linear oscillating flow in a homeoplanar cell*

The oscillating flow in a weakly anchored LC cell is restricted now to the case of linear director motion in the plane of the flow [18, 19]. This case is not easy to realize experimentally. Indeed, Poiuseulle flow produces certain destabilizing moments, which can induce LC director deviation out of the flow plane. Such instability was predicted and experimentally studied for both stationary and oscillating flows in the case of strong homeotropic alignment [25, 26, 28]. The instability occurs at a certain threshold amplitude of the pressure gradient. It was shown theoretically that, for a steady flow, LC weak anchoring (both in polar and azimuthal directions) decreases the threshold of such an instability [29]. Such an effect is quite possible in our cell in spite of the stabilizing action of the substrate with weak planar anchoring. So in our experiments we also controlled the optical response of the cells in geometry 'b' (see above) to be sure location of the LC director in the flow plane. Indeed, we observed that the optical response in geometry 'b' arose at some threshold amplitude of the pressure gradient, depending on the frequency of the oscillations. The results described in this paper were obtained at pressure gradients lower than this threshold value. To provide a better understanding of the problem we also present some analogous data for a linear regime in a homeotropic LC cell filled with MBBA.

The time dependence of light intensity passing through the LC cell subjected to pressure oscillations is shown in figures 10 (*a*) and 10 (*b*). We see that at high frequency (low period) of the pressure variations the sensitivity of the LC layer decreases and a quasi-harmonic optical response appears with the same frequency as the pressure oscillations, figure 10 (*a*). In the case of initial homeotropic alignment, the LC optical response occurs at the corresponding double frequency, figure 11 (*a*).

At low frequency a considerable distortion of $I(t)$ dependence can take place, figure 10 (*b*), even for relatively small values of the pressure difference amplitude. The same was observed in a hometropic layer of MBBA, figure 11 (*b*), and takes place due to the increase of sensitivity of the LC cell at low frequency and the complicated dependence of the intensity of light on the phase delay (23). In this case the maximum value of the light intensity, I_0, is needed to find the phase delay δ. As shown in [20], for a linear regime of a director motion this parameter is approximately proportional to the mean value of the squared polar angle

Downloaded At: 15:53 25 January 2011

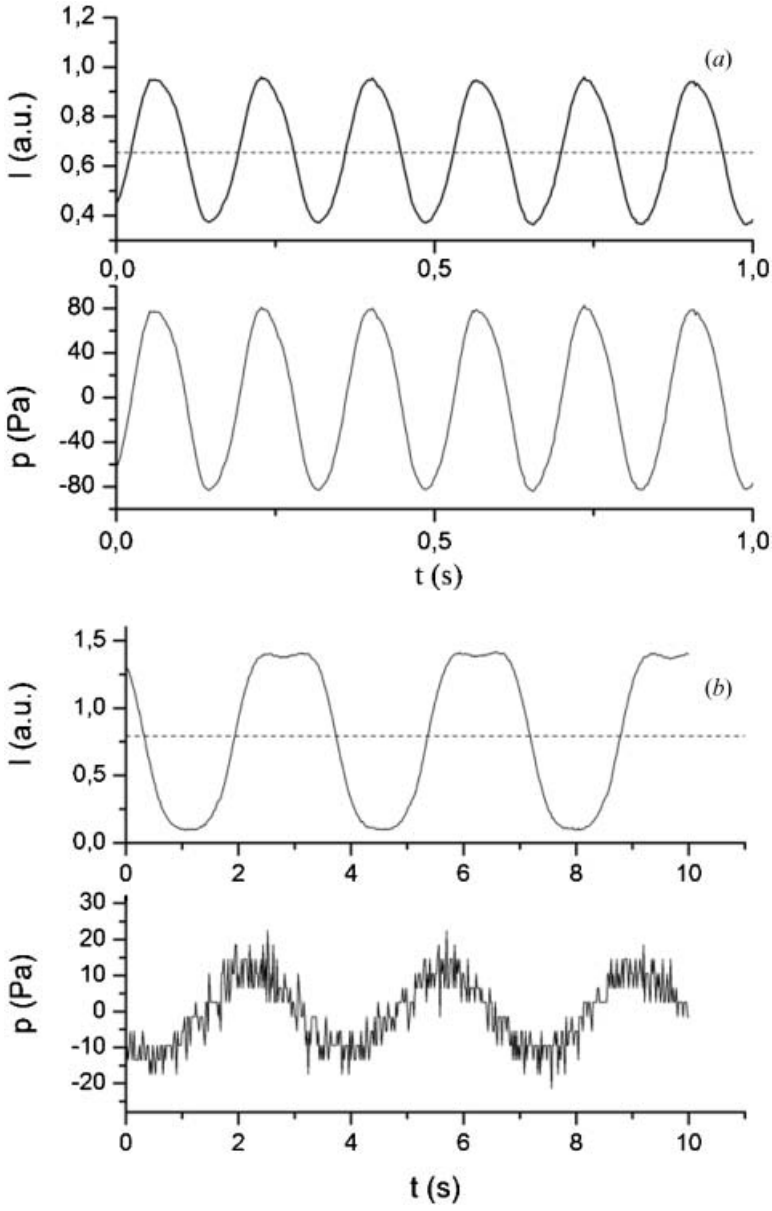

Figure 10. Optical response $I(t)$ of a hybrid layer of ZhK616 on the oscillating pressure difference Δp; $d=20\,\mu m$, $t_{ex}=10\,min$. (*a*) $T=0.165\,s$, $\Delta p_0=81.0\,Pa$, $\Delta\delta=0.70\,rad$; (*b*) $T=3.43\,s$, $\Delta p_0=19\,Pa$, $\Delta\delta=3.48\,rad$. Dotted lines correspond to the light intensity without flow.

and thus to the squared pressure amplitude. Experimental dependences $\delta_m(\Delta p^2{}_0)$ presented in figure 12 confirm this theoretical prediction.

The existence of the initially deformed structure in the homeoplanar cell results in the non-symmetric response shown in figure 10 (*b*). In this case the difference $\widetilde{\delta}$ between maximum δ_{max} and minimum δ_{min} values of the phase delay can be used instead of δ_{max}. In contrast to the case of homeotropic orientation, this parameter depends linearly on the amplitude of the pressure difference applied to the cell, at least at low values of its amplitude and frequency, figures 13 (*a*) and 13 (*b*). Some non-linear distortions take place at sufficiently high values of frequency. The sensitivity of this dependence to thickness variation figure 13 (*b*), at a frequency of 10 Hz ($T=0.1\,s$) is weaker than for low frequency data obtained for strong homeotropic anchoring, figure 12.

Examples of the frequency dependence of a normalized phase delay difference $\widetilde{\delta}\big/(\Delta p_0/\Delta x)$ under variable experimental conditions are shown in figure 14. There is no essential difference for the curves obtained at

Downloaded At: 15:53 25 January 2011

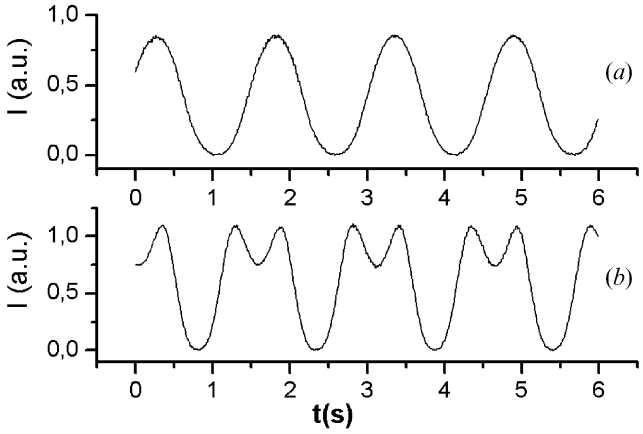

Figure 11. Optical response $I(t)$ of a homeotropic layer of MBBA. $T=3.1$ s, $d=112\,\mu$m, $L=0.01$ m. (*a*) $\Delta p_0/\Delta x=5.5\times10^3\,\mathrm{Pa\,m^{-1}}$, $\delta_m=2.18$ rad; (*b*) $\Delta p_0/\Delta x=7.7\times10^3\,\mathrm{Pa\,m^{-1}}$, $\delta_m=4.3$ rad.

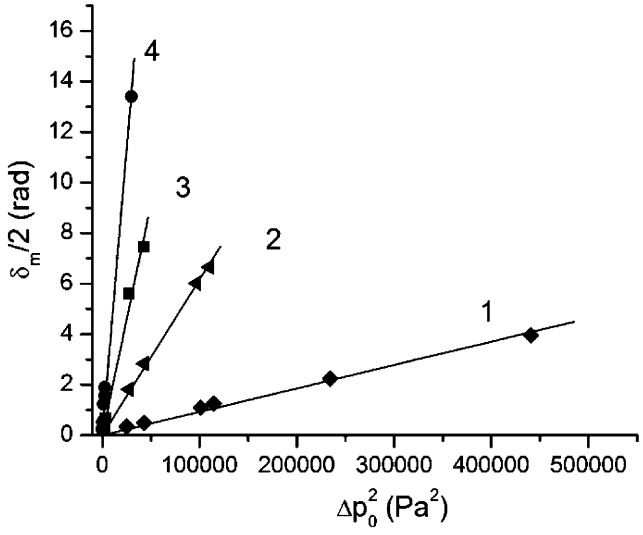

Figure 12. Dependence of phase difference δ_m on the squared pressure amplitude Δp_0 in MBBA for various layer thicknesses. Symbols, experimental results, lines, approximation by linearization. $T=3.2$ s, 1, $d=25.4\,\mu$m, 2, $d=29.6\,\mu$m; 3, $d=32.8\,\mu$m; 4, $d=37.6\,\mu$m.

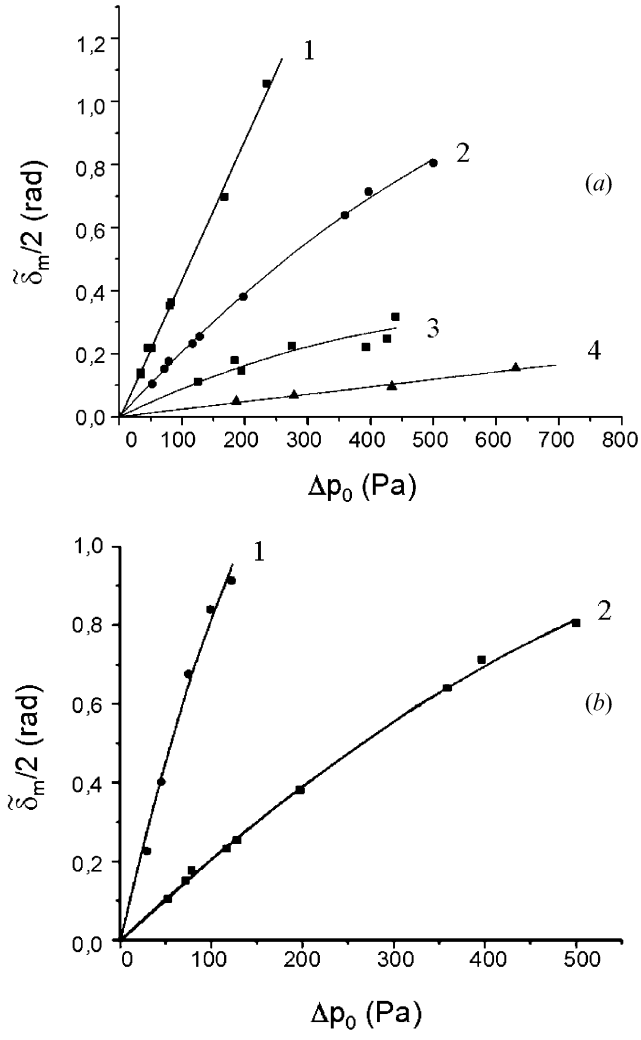

Figure 13. Dependence of flow induced variations of phase delay $\tilde{\delta}_m$ in a hybrid cell on the pressure difference amplitude Δp_0, (*a*) ZhK616, $d=20\,\mu$m, $t_{ex}=10$ min; 1, $T=0.14$ s, 2; $T=0.10$ s; 3, $T=0.0640$ s; 4, $T=0.040$ s; (*b*) ZhK616, $T=0.10$ s; 1, $d=42.3\,\mu$m; 2, $d=20\,\mu$m. Solid lines denote polynomial approximation of the second order.

different exposure times of UV treatment t_{ex}. So fast surface dynamics is insensitive to this parameter at least in our experimental conditions.

There is some tendency for a decrease in the mean slope of the curves for thinner LC layers. This can be considered as a weak influence of the surface viscosity, as this would be more pronounced at lower thickness values. Nevertheless, comparison between the experimental and calculated frequency dependences of the phase delay differences at low LC thickness does not lead to the value of the surface viscosity coefficient, because the sensitivity of the calculated curves to changes of anchoring energy (figure 5) is considerably higher than to variation in the surface viscosity coefficients (figure 6). Our estimates show that the thickness of the boundary layer corresponding to the surface viscosity does not exceed 10^{-6} m. For more precise information on the surface viscosity coefficient for surfaces with relatively weak anchoring, one has to increase the frequency of oscillations and decrease the thickness of the LC layer. Moreover, more precise measurements of polar anchoring strength are required to find reasonable values of the LC surface viscosity. Indeed, this can be done using the technique described above at extremely low frequencies of oscillations, when

Downloaded At: 15:53 25 January 2011

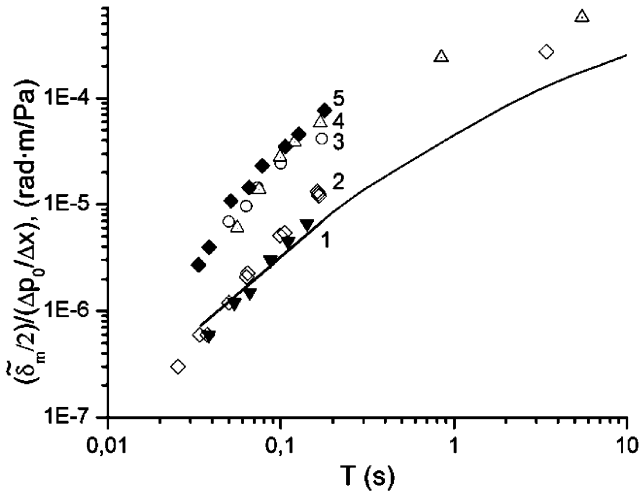

Figure 14. Normalized difference of phase delay as a function of pressure oscillation period in ZhK616. $d=20\,\mu m$: 1, $t_{ex}=20\,min$; 2, $t_{ex}=10\,min$, $d=45\,\mu m$: 3, $t_{ex}=10\,min$; 4, $t_{ex}=20\,min$; 5, $t_{ex}=40\,min$. Symbols, experimental data; line, theoretical curve (numerical calculations for $l_{\gamma_1}=10^{-7}\,m$, $W=10^{-7}\,J\,m^{-2}$, the parameters of MBBA were used).

surface viscosity effects can be neglected. Our experimental method can also be used to study fast surface dynamics with weak anchoring provided by an alternative surface treatment [30].

5. Conclusion

In this paper we present the first experimental study of linear oscillating Poiseuille flow of a nematic LC in a hybrid cell; this combines a surface with strong homeotropic anchoring and a surface with a planar boundary orientation induced by UV-light, and a LC cell with a strong homeotropic anchoring. It was shown that at a relatively low pressure gradient, the LC director moves in the plane of the flow in both cases, which simplifies the theoretical description of the problem. The optical response of hybrid and homeotropic LC cells under an oscillating pressure gradient was investigated, with variation of amplitude and frequency of the pressure gradient. The linear hydrodynamic equations were solved analytically for symmetrical boundary conditions and compared with experimental results for the initially homeotropic layer distorted by the oscillating pressure gradient. This solution was also obtained numerically for the general case of weak planar anchoring involving a finite value of the polar anchoring strength and a non-zero value of the surface viscosity coefficient. It was shown that in the frequency range 0.1–10 Hz, and for a LC layer thickness of about 20 μm and anchoring strength of about $10^{-7}\,J\,m^{-2}$, the optical response is almost independent on surface viscosity when the thickness of the boundary layer responsible for this parameter does not exceed $10^{-6}\,m$. For surfaces with intermediate anchoring strength (as in our case) a more precise value of the surface viscosity can be obtained by use of thinner LC cells with a simultaneous increase of the oscillation frequency. The results obtained show that the proposed technique of linear oscillating Poiseuille flow shows promise in the study of fast surface dynamics of liquid crystals.

Acknowledgements

This research was supported by HKUST RGC grant 6149/04E and DAG grant O5/06.EG14.

References

[1] V.G. Chigrinov. *Liquid Crystal Devices: Physics and Applications*. Artech House, Boston (1999).
[2] F.S.Y. Yeung, H.S. Kwok. *Appl. Phys. Lett.*, **83**, 4291 (2003).
[3] G.P. Crawford, D.K. Yang, S. Zumer, D. Finotello, J.W. Doane. *Phys. Rev. Lett.*, **66**, 723 (1991).
[4] J.-P. Korb, L. Malier, F. Cros, X. Shu, D.J. Jonas. *Phys. Rev. Lett.*, **77**, 2312 (1996).
[5] B.Y. Derjaguin, Yu.M. Popovskij, B.A. Altoiz. *J. Colloid Interface Sci.*, **96**, 492 (1983).
[6] V.P. Vorflusev, H.S. Kitzerow, V.G. Chigrinov. *Appl. Phys. Lett.*, **70**, 3359 (1997).
[7] E.A. Oliveira, A.M. Figueiredo, G. Durand. *Phys. Rev. A*, **44**, R825 (1991).
[8] S. Faetti, M. Nobili, I. Raggi. *Eur. Phys. J. B*, **11**, 445 (1999).
[9] V.I. Tsoy. *Mol. Cryst. liq. Cryst.*, **264**, 51 (1995).
[10] I. Jánossy, T.I. Kósa. *Phys. Rev. E*, **70**, 052701 (2004).
[11] S.V. Pasechnik, V.G. Chigrinov, D.V. Shmeliova, et al. *IDMC Digest*, 593 (2005).
[12] G.E. Durand, E.G. Virga. *Phys. Rev. E*, **59**, 4137 (1999).
[13] P.J. Kedney, F.M. Leslie. *Liq. Cryst.*, **24**, 613 (1998).
[14] A.G. Petrov, A.Th. Ionescu, C. Versache, N. Scaramuzza. *Liq. Cryst.*, **19**, 169 (1995).
[15] M. Vilfan, I. Drevensek, A. Mertelj, M. Copic. *Phys. Rev. E.*, **63**, 061709 (2001).
[16] A. Mertelj, M. Copic. *Phys. Rev. Lett.*, **81**, 5844 (1998).
[17] V. Chigrinov, S. Pikin, A. Verevochnikov, et al. *Phys. Rev. E*, **69**, 061713 (2004).
[18] I.Sh. Nasibullaev, A.P. Krekhov. *Crystallogr. Rep.*, **46**, 540 (2001).
[19] M.V. Khazimulin, T. Borzsonyi, A.P. Krekhov, et al. *Mol. Cryst. liq.Cryst.*, **329**, 247 (1999).
[20] S.V. Pasechnik, A.V. Torchinskay. *Mol. Cryst. liq. Cryst.*, **341**, 331 (1999).
[21] S.V. Pasechnik, A.V. Torchinskay, D.V. Shmeliova, T.N. Yurmanova. *Mol. Cryst. liq. Cryst.*, **409**, 449 (2004).
[22] P.P. Karat, N.V. Madhusudana. *Mol. Cryst. liq. Cryst.*, **36**, 51 (1976).
[23] H. Kneppe, F. Schneider. *Mol. Cryst. liq. Cryst.*, **65**, 23 (1981).
[24] H. Kneppe, F. Schneider. *J. Phys. E: sci. Instrum.*, **16**, 512 (1983).

Downloaded At: 15:53 25 January 2011

[25] S.V. Pasechnik, A.P. Krekhov, D.V. Shmeliova, et al. *JETP*, **100**, 804 (2005).
[26] A.P. Krekhov, T. Borzsonyi, P. Toth, et al. *Phys. Rep.*, **337**, 171 (2000).
[27] See, for example, V. Chigrinov, A. Muravski, H.S. Kwok, et al. *Phys. Rev. E*, **68**, 061702 (2003).
[28] O.S. Tarasov, A.P. Krekhov, L. Kramer. *Mol. Cryst. liq. Cryst.*, **328**, 573 (1999).
[29] O.S. Tarasov, A.P. Krekhov, L. Kramer. *Liq. Cryst.*, **28**, 833 (2001).
[30] L.T. Thieghi, R. Barberi, J.J. Bonvent, et al. *Phys. Rev. E*, **67**, 041701 (2003).

Downloaded At: 15:53 25 January 2011